

# Multiple Outflows in the Giant Eruption of a Massive Star<sup>1</sup>

Roberta M. Humphreys<sup>2</sup>, John C. Martin<sup>3</sup>, Michael S. Gordon<sup>2</sup>, and Terry J. Jones<sup>2</sup>

## ABSTRACT

The supernova impostor PSN J09132750+7627410 in NGC 2748 reached a maximum luminosity of  $\approx -14$  mag. It was quickly realized that it was not a true supernova, but another example of a non-terminal giant eruption. PSN J09132750+7627410 is distinguished by multiple P Cygni absorption minima in the Balmer emission lines that correspond to outflow velocities of -400, -1100, and -1600 km s<sup>-1</sup>. Multiple outflows have been observed in only a few other objects. In this paper we describe the evolution of the spectrum and the P Cygni profiles for three months past maximum, the post-maximum formation of a cool, dense wind, and the identification of a possible progenitor. One of the possible progenitors is an infrared source. Its pre-eruption spectral energy distribution suggests a bolometric luminosity of -8.3 mag and a dust temperature of 780°K. If it is the progenitor it is above the AGB limit unlike the intermediate luminosity red transients. The three P Cygni profiles could be due to ejecta from the current eruption, the wind of the progenitor, or previous mass loss events. We suggest that they were all formed as part of the same high mass loss event and are due to material ejected at different velocities or energies. We also suggest that multiple outflows during giant eruptions may be more common than reported.

*Subject headings:* stars: massive – supernovae: – variables: – winds,outflows

---

<sup>1</sup>Based on observations obtained with the Large Binocular Telescope (LBT), an international collaboration among institutions in the United States, Italy and Germany. LBT Corporation partners are: The University of Arizona on behalf of the Arizona university system; Istituto Nazionale di Astrofisica, Italy; LBT Beteiligungsgesellschaft, Germany, representing the Max-Planck Society, the Astrophysical Institute Potsdam, and Heidelberg University; The Ohio State University, and The Research Corporation, on behalf of The University of Notre Dame, University of Minnesota and University of Virginia.

<sup>2</sup>Minnesota Institute for Astrophysics, 116 Church St SE, University of Minnesota, Minneapolis, MN 55455; roberta@umn.edu

<sup>3</sup>University of Illinois Springfield, Springfield, IL 62703

## 1. Introduction

Transient surveys are finding an increasing number of what appear to be non-terminal giant eruptions. Many of these giant eruptions are spectroscopically similar to Type IIn supernovae and thus receive a supernova (SN) designation, but are later recognized as sub-luminous or their spectra and light curves do not develop like true supernovae. Consequently, they are often referred to as “supernova impostors” (Van Dyk et al. 2000). These impostors or giant eruptions are examples of high mass loss episodes apparently from evolved massive stars (see Van Dyk & Matheson 2012 for a review and references therein). Authors often refer to them as Luminous Blue Variables (LBVs), but these giant eruptions are distinctly different from LBV/S Doradus variability in which the star does not increase in luminosity and the eruption or maximum light can last for several years.

PSN J09132750+7627410 did not receive a supernova designation. It was posted on the CBAT Transient Objects Confirmation Page on 2015 February 10 by K. Itagaki as a possible supernova (PSN) in NGC 2748. The first reported magnitudes of 17.7 to 18.1 suggested a luminosity of  $\approx -14$  mag based on membership in NGC 2748 at a mean distance of 20.97 Mpc via NED, and based on Tully-Fisher and kinematic distances. Thus, it was likely not a true supernova, but another example of a giant eruption. A spectrum obtained only a day later, on 2015 February 11 reported by Tartaglia, et al. (2015) showed narrow emission lines. They also measured an apparent V magnitude of 18.7 and a luminosity of -13 mag. Based on the spectral appearance and the luminosity, they suggested that this PSN was a SN impostor.

Our first spectrum of PSN J09132750+7627410 (Humphreys & Gordon 2015) observed on 2015 February 16, showed multiple P Cygni absorption components in the prominent Balmer emission lines. These features could be due to ejecta from the current eruption, from previous mass loss events, or the wind of the progenitor. Evidence for multiple outflows have been previously observed in the spectra of only a few objects; two impostor eruptions (SN2000ch, SN Hunt 248), the peculiar SN2009ip, and a Type IIn supernova (SN2005gj), see §4. For that reason we obtained additional spectra and photometry. In this brief *Paper* we present our observations, describe the spectrum and our measurements, discuss a possible progenitor, and the origin of the multiple P Cygni absorption features.

## 2. Observations

### 2.1. Spectroscopy

Moderate resolution spectra of PSN J09132750+7627410 were observed with the MODS1 spectrograph on the Large Binocular Telescope (LBT) in February, April and May, 2015. The MODS1 uses a dichroic to obtain blue and red spectra simultaneously with the G400L and G750L gratings, respectively. The total wavelength coverage is from 3200Å to more than 1 $\mu$ m. We used a 1" slit yielding a resolution of 1500 in the blue and 2000 in the red. This gives a velocity resolution of 150 km s<sup>-1</sup> at H $\alpha$ . The two dimensional spectra were initially reduced using the *modsCCDred* pipeline for bias subtraction and flat fielding. The spectra were then extracted, and wavelength and flux calibrated using the standard IRAF twodspec and onedspec packages. The extracted spectra cover the wavelength ranges 3600 – 5600 and 6000 – 9000 Å. The MODS1 uses standard lamps exposed during the afternoon for wavelength calibration, but despite a flexure model, there remain wavelength calibration uncertainties. For this reason we used the night sky lines for the wavelength calibration in the red. This may introduce a small velocity offset between the blue and red spectra. But, for this object in NGC 2748 (velocity +1476 km sec<sup>-1</sup>), the difference is not significant for our discussion.

The journal of observations is given in Table 1.

### 2.2. Photometry During the Eruption

Broadband CCD photometry with ASTRODON Johnson-Cousins filters was obtained with the 20-inch telescope at the Barber Observatory with an Apogee U42 CCD camera using a back-illuminated E2V CCD42-40 chip. All images were flat-fielded and bias and dark subtracted. Aperture photometry was measured using VPHOT (<https://www.aavso.org/vphot>) developed primarily by Geir Klingenberg (coding and design) and Arne Henden (photometry). Photometry was measured in circular apertures with a diameter 3.0 times the FWHM of the stellar profiles. Sky background was sampled from an annulus centered on each star with an inner radius of 11.5" and 3" wide. No effort was made to subtract the underlying contribution from the galaxy. The galaxy contribution is estimated from images without the target present to be  $V = 21$  mag arcsec<sup>-2</sup> (about  $V = 19$  mag in a typical aperture).

The brightness of the target is an unweighted average measured with respect to 9 reference stars in the magnitude range  $V = 14.0$  to 16.2 and within 10 arcminutes of the galaxy (but well separated from it) selected from the UCAC4 catalog (Zacharias et al. 2013) using

the prescription of Toone (2005). Photometric error for the target was calculated as the quadrature sum of the CCD equation noise for the target, plus the standard deviation of the reference stars. We used the standard photometric transformations for the optical system.

The photometric observations are summarized in Table 2 which also includes the discovery magnitudes from the CBAT Transient Objects Followup Reports. The earliest photometry observed during the first 24hrs shows a decline of 0.6 mag which could be due to a difference in calibration. We note though that the early I band magnitude is consistent with later photometry. Additional post-maximum magnitudes were recorded in the Pan-STARRS Survey for Transients. The target is PS15jf. The r(P1) and i(P1) magnitudes in Table 2 are on the Pan-STARRS filter system (Tonry et al. 2012).

Although the photometric record is sparse, and the onset of the eruption is uncertain, the available data suggest that this eruption was relatively brief. PSN J09132750+7627410 was at or near maximum light for only about a month. The photometry shows that a decline had begun by about 30 days post-maximum. Interestingly, our data point from 2015 May 19 suggests that the object may have brightened somewhat. This is supported by the flux-calibrated spectrum from May 20 observed under good conditions. Short-term oscillations in brightness are common in these objects as is evident from the erratic behavior of SN2009ip (Pastorello et al. 2012; Margutti et al. 2014; Martin et al. 2015). To check on variability and a possible recovery, we observed it again in 2016 January and February. The target remained below our limit of detectability defined as the median value in the aperture that was not statistically different from the median value in the background annulus. We note that the seeing and observing conditions were excellent for the February measurement.

### 2.3. Pre-Eruption Images and a Possible Progenitor

NGC 2748 is a well-studied spiral galaxy at a distance of 20.97 Mpc, modulus 31.60 mag, from NED. It is the site of a super-massive black hole in its nucleus and two previous supernovae, SN1985A (Ia) and SN2013ff (Ic). Consequently, there are numerous space-based images in the Mikulski Archive for Space Telescopes (MAST), but PSN J09132750+7627410 is in the outer parts of the galaxy, and was just off the frame in most of the *HST* images. We identified the target field on four *HST*/WFPC2 images of NGC 2748; two with F450W and two with F814W. (GO-9042,PI:Smartt) obtained 2001 July 6. The exposure times were 230s each and the target was on the WF3 chip. We processed the images using DOLPHOT (Dolphin 2000) which successfully fit a PSF to six objects within 2'' of the target position with sigma threshold 2.5, the default. We only considered DOLPHOT detections consistent with a point source (class 1 and 2) using the default WFPC2 DOLPHOT settings. Only

two objects were above the sky background in all four images. The resulting photometry in VEGAMAGs for these two objects is in Table 3. The F450W and F814W filters are comparable to the Johnson B and Cousins I bands, respectively, yielding an instrumental F450W -F814W or  $b-i$  color.

For comparison with the target’s published position, which we confirmed with astrometry from our CCD images<sup>1</sup>, we determined the offsets of their WCS image centers relative to ICRS J2000 coordinates using four GSC 2.3 stars on the same frame, shifted in X and Y and with rotation with a standard deviation of  $0''.4$  in RA and Dec. The combined uncertainty of the target’s position and of the WCS in the HST image is then  $0''.45$ . Their ICRS positions are included in Table 3. The two summed HST frames are shown in Figure 1, centered on the impostor’s position and corrected for the offset. Star A is within the small circle, radius  $0''.2$ , centered on the target’s position. The fainter star B, further from the center, is just outside a circle with the  $0''.45$  radius. It is apparently quite red, but with a large uncertainty. Based on its position, star A is the more likely progenitor. Its absolute blue magnitude (F450W) would be  $\approx -7.3$ , with a foreground galactic extinction  $A_B$  of 0.097 (Schlafly & Finkbeiner 2011). Its extinction-corrected  $b-i$  color of 0.58 mag implies an A-type or early F-type supergiant. NGC 2748 has prominent dust lanes, although none are apparent close to the target, so there may be some additional internal extinction and star A would be both brighter and bluer. There is also an extended area of low level emission around star A visible in the F814W image which could be due to unresolved stars.

We have also identified a source in the Spitzer Science Archive in three separate epochs at  $3.6\mu\text{m}$  and  $4.5\mu\text{m}$  at nearly the same position. Since the background is high and variable, we initially used a profile fitting routine to determine the flux distribution across the image and the appropriate radius for aperture photometry. We then used the Astropy-affiliated package “photutils” to measure aperture photometry on the Level 2 PBCD mosaic images. Since there is a significant gradient in the infrared background, particularly in the  $4.5\mu\text{m}$  images, the sky is modeled as a two-dimensional polynomial surface across the source and subtracted from a  $1.8''$  radius aperture. In each image, subpixel centroids are calculated as the center of mass determined from image moments. The magnitudes are included in Table 3 with errors calculated from the uncertainty maps provided by the Spitzer Science Archive for each field. The IRAC images from 2014 have the best signal to noise and are shown with the HST/WFPC2 F814W image for comparison in Figure 2. We found no systematic offset between the the IRAC position and the ICRS J2000 using the same reference stars, but with

---

<sup>1</sup>We measured an average position of RA 09:13:27.55, Dec +76:27:41.1 in ICRS J2000 coordinates with a standard deviation of  $0''.2$  from six separate images using GSC 2.3 stars in the field with astrometry.net (Lang et al. 2010). This agrees very well with the discovery position.

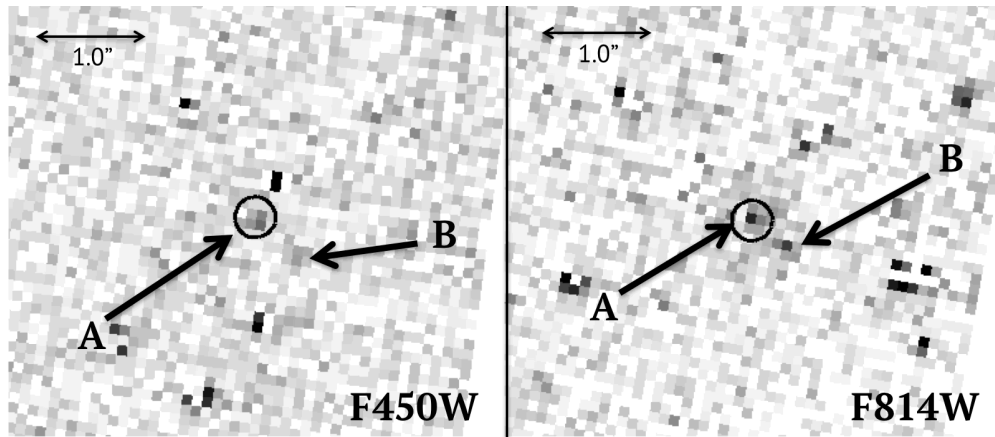


Fig. 1.— The summed HST/WFPC2 F450W and F814W images including the region around PSN J09132750+7627410. The smaller dashed circle  $0''.2$  in radius is centered on the position of the impostor. The cosmic rays have not been removed.

a standard deviation of  $0''.64$  and  $0''.46$  in RA and Dec respectively. The WFPC2 and IRAC frames are thus on the same coordinate system. The IRAC position is included in Table 3. We were not able to identify the source in the WISE survey, because it is not resolvable from the background galaxy.

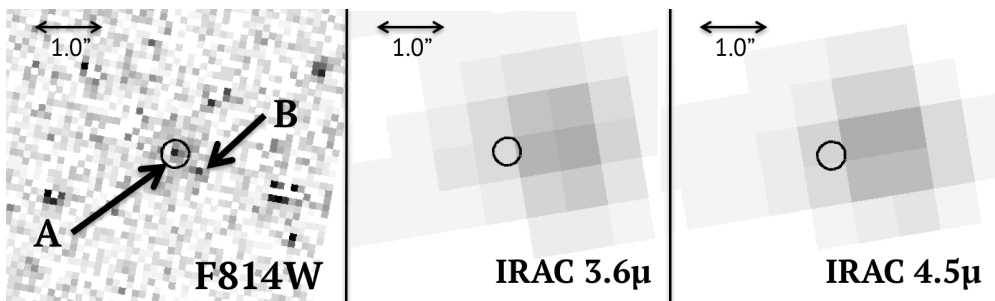


Fig. 2.— The HST/WFPC2 F814W image and IRAC  $3.6\mu\text{m}$  and  $4.5\mu\text{m}$  images from 2014 of the region around PSN J09132750+7627410. The WCS coordinates were corrected to the ICRS J2000 using the same reference stars so that the WFPC2 and IRAC frames are on the same coordinate system..

The spectral energy distributions (SED) are shown in Figure 3 for stars A and B and the IRAC source. The IRAC source is very red with a rising energy distribution to longer wavelengths similar to obscured AGB stars and OH/IR stars (Jones et al. 1982) with extensive circumstellar dust. Without longer wavelength data it is not possible to know where the SED peaks. We show Planck curves fits to the data points from 2014 with a color tem-

perature of 780°K. The source could be both cooler and more luminous. Planck curves are also shown fit to the optical photometry for stars A and B.

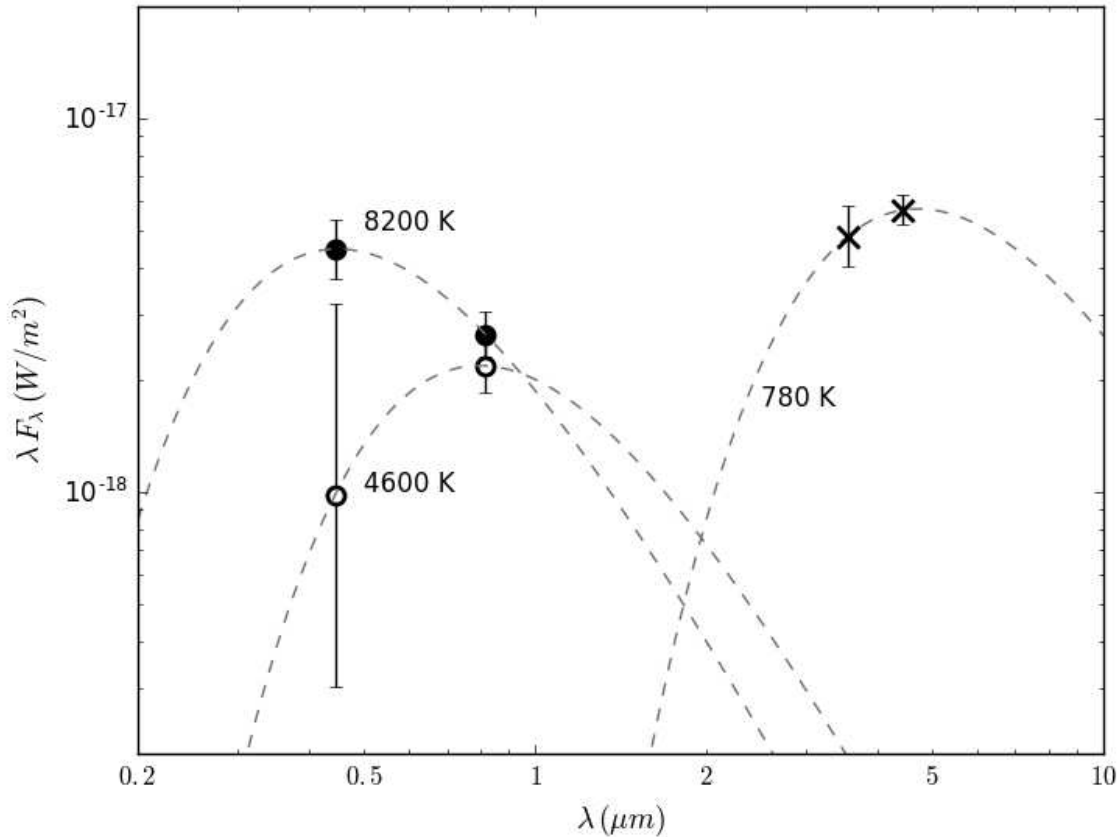


Fig. 3.— The SEDs for stars A and B and the infrared source near the position of PSN J09132750+7627410. Planck curve fits are shown with color temperatures of 8200°K and 4600°K for stars A , filled circles, and B, open circles, and 780°K for the infrared source. No corrections for possible interstellar extinction have been applied.

We have two possibilities for an optical progenitor; star A or B, alone or in combination with the infrared source. The photometry for star A is incompatible with the IR SED. If A is the progenitor, it would be an intermediate-type supergiant of relatively low luminosity ( $9 \times 10^4 L_\odot$ ,  $M_{Bol} = -7.6$  mag) and initial mass  $\approx 15 - 20 M_\odot$ . Star B has a luminosity of  $4.4 \times 10^4 L_\odot$  and based on its somewhat uncertain color, it could be an evolved star of approximately  $12 - 15 M_\odot$ . Based on these limited SEDs, it is possible that the infrared source could be associated with star B. If so, then star B’s luminosity would be dominated by the infrared radiation.

Given the lower spatial resolution with IRAC, another possibility is that the infrared source, possibly with no optical counterpart, is the progenitor. The positions of the impostor and the IRAC source marginally agree at the 1 sigma level and are coincident within two sigma of their positional uncertainties. If this is the case, PSN J09132750+7627410 could be similar to the dusty Intermediate Luminosity Red Transients (ILRTs) like SN 2008S (Smith et al. 2009) and the 2008 NGC 300 OT (Bond et al. 2009; Humphreys et al. 2011). Assuming that the infrared source is similar to an AGB, we use its  $3.6\mu\text{m} - 4.5\mu\text{m}$  color index in 2014 with the bolometric calibration from Blommaert et al. (1998) to derive a bolometric magnitude of -8.3 mag ( $1.6 \times 10^5 L_{\odot}$ ). Integrating the Planck curve gives a luminosity of  $10^5 L_{\odot}$ . This luminosity is well above the nominal AGB limit at  $M_{Bol} \cong -7.0$  mag. The object is more luminous and therefore more massive than the ILRTs which are close to the AGB limit, see the HR diagram (Fig. 14) in Humphreys et al. (2011). It is too red to be a foreground dwarf. Alternatively, it could be an H II region or the chance superposition of a background object such as an AGN, but we could not find any catalogued objects at its position.

Assuming that the infrared source is in NGC 2748, with this luminosity, the candidate would of course be a massive star of  $\approx 25 M_{\odot}$ . It could be a very dusty red supergiant perhaps similar to the OH/IR stars in our galaxy. They are potential supergiants, but their distances are not known. Thompson, et al. (2009) and Khan, et al. (2015) have identified several luminous, optically obscured stars in M33 and other nearby galaxies which may be similar to the supergiant OH/IR stars. The infrared source’s mid-infrared color and dust temperature are similar to many of the sources listed by Khan, et al. (2015), although their objects are significantly more luminous with  $\log L \sim 5.5$  to  $6.0 L_{\odot}$ .

It is tempting to identify the infrared source with the erupting star, but more information was needed. Time was requested with Spitzer to confirm if the IRAC source had survived or changed after the eruption, but was denied. Based on their positions, stars A and B and the infrared source are all possible progenitors, but we favor a tentative identification with the infrared source.

If the infrared source is the progenitor, the underlying star is most likely a cool or intermediate temperature evolved supergiant that may be transiting the HR Diagram to the blue, similar to more luminous examples such as VarA in M33. In this transition, the stars enter a period of enhanced instability that leads to high mass loss episodes. Followup imaging of PSN J09132750+7627410 with HST and Spitzer would be very worthwhile.



### 3. The Spectrum: Multiple P Cygni Absorptions

Our first and highest quality spectra from 2015 February 16 were observed about six days after the reported discovery and the presumed maximum. The blue spectrum is shown in Figure 4. The blue and red spectra show strong narrow Balmer emission lines with prominent P Cygni features from  $H\alpha$  to  $H\epsilon$ . Three absorption minima are present in  $H\beta$ ,  $H\gamma$ ,  $H\delta$  and at least two are clearly identified in  $H\alpha$ . The  $H\alpha$  and  $H\beta$  profiles are shown in Figure 5 with the multiple absorption minima identified. In addition to the narrow peaks, the hydrogen emission profiles all show the classic asymmetric Thomson scattering profile with prominent red wings extending to more than  $2000 \text{ km s}^{-1}$  at  $H\alpha$  and  $H\beta$  due to scattering off the electrons in the wind not Doppler motion. Because of the strong scattering wings, we measured the widths of the  $H\alpha$  and  $H\beta$  lines above where the profile begins to broaden. The “FWHM” of the  $H\alpha$  and  $H\beta$  narrow peaks are  $379 \text{ km s}^{-1}$  and  $368 \text{ km s}^{-1}$ , respectively<sup>2</sup>. The narrow Balmer emission peaks have a mean velocity of  $1685 \text{ km s}^{-1}$ , and the individual lines show no significant velocity shift in the two later spectra. Although, this is about  $200 \text{ km s}^{-1}$  greater than the published Doppler velocity for NGC 2748 of  $+1476 \text{ km s}^{-1}$ , the object is in the outermost parts of the galaxy, and the velocity difference is consistent with rotation at its distance from the center (Atkinson et al. 2005).

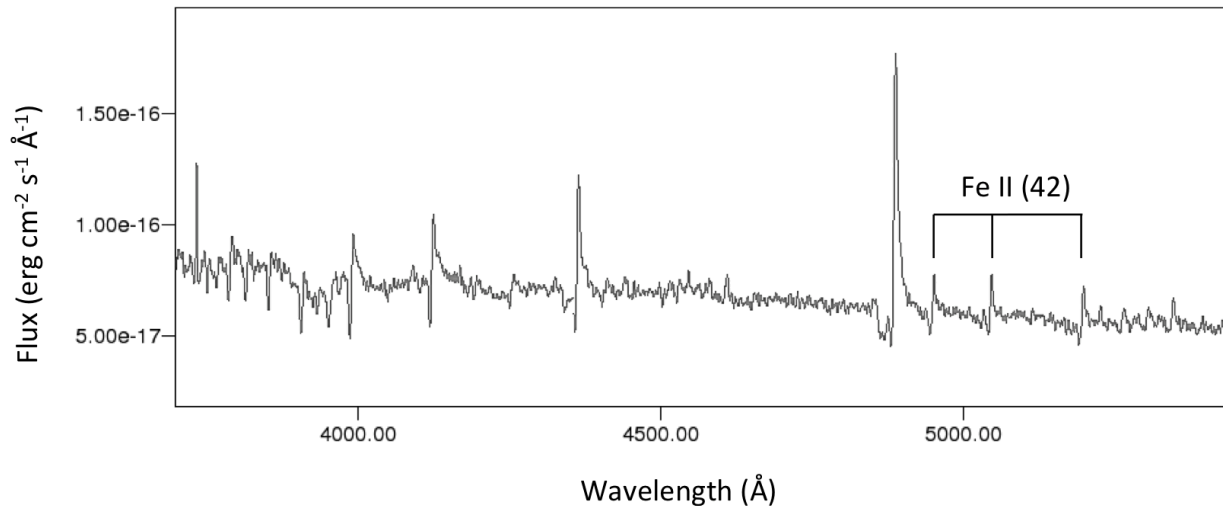


Fig. 4.— Blue spectrum from day 6

The higher Hydrogen lines at  $\lambda\lambda$  3889, 3835, 3797, and 3770 Å are clearly visible in

---

<sup>2</sup>The FWHM was measured at  $1.62 \times 10^{-16} \text{ ergs s}^{-1} \text{ cm}^{-2} \text{ Å}^{-1}$  for  $H\alpha$  and at  $1.25 \times 10^{-16} \text{ ergs s}^{-1} \text{ cm}^{-2} \text{ Å}^{-1}$  for  $H\beta$

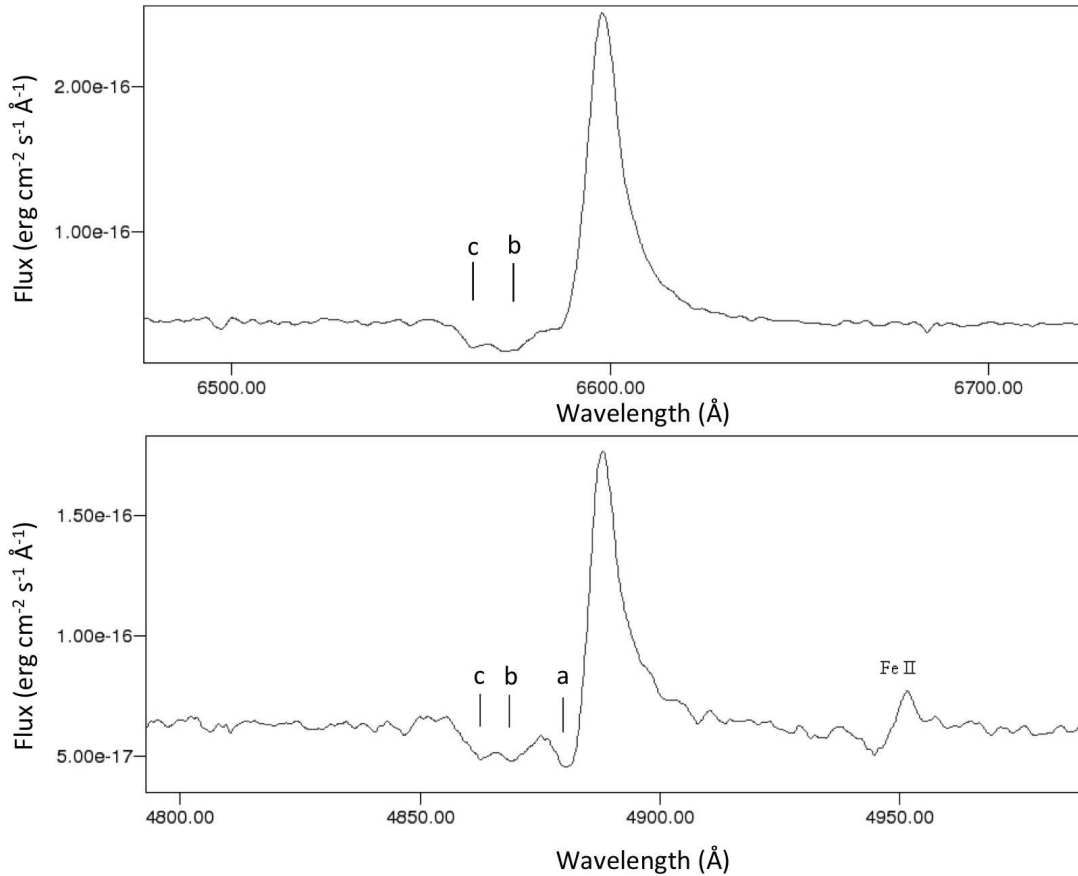


Fig. 5.— The profiles of the H $\alpha$  (top) and H $\beta$  (bottom) lines from Day 6 showing the multiple P Cygni absorption features.

absorption and are blue-shifted relative to the Balmer emission lines by about  $300 \text{ km s}^{-1}$  which we attribute to formation in the expanding wind or ejecta. The Fe II multiplet 42 lines are also prominent in emission with strong P Cygni absorption features, but with no more than one absorption minimum, blue-shifted by about  $400 \text{ km s}^{-1}$  relative to the peak emission. So the Fe II absorption is not formed in the faster moving ejecta. Numerous other Fe II lines are present in emission but without P Cygni profiles. The Ca II K absorption line is present, and in the red, the strong, luminosity sensitive O I triplet at  $\lambda 7774 \text{ \AA}$  is in absorption.

The first low-resolution spectrum described by Tartaglia, et al. (2015) and observed within 24 hours of the discovery, does not show the multiple P Cyg absorptions. Our first spectrum was obtained only five days later, and although the difference could be real, we

attribute it to the difference in spectral resolution,  $14 \text{ \AA}$  vs.  $3 \text{ \AA}$  in our spectra. The total width of the P Cyg absorption feature is the same in both spectra.

All of the line identifications and measured velocities discussed in this section are given in Table 4. Although, it is common to quote the terminal velocity ( $v_\infty$ ) for the P Cygni profiles of hot stars, the terminal velocity, however, is derived from a stellar wind model fit to the profiles of resonance lines. The Hydrogen lines are not resonance lines. We also chose not to fit Gaussians to determine the blue edge velocity because of the reduced S/N in some of the spectra together with the complex profiles with multiple minima plus the strong scattering wings. Instead, we give the velocity at the absorption minimum measured relative to the emission peak which permits a well-controlled differential measurement.

When our second spectrum was observed on Day 71, PSN J09132750+7627410 had already faded significantly. The blue spectrum has very poor S/N, and only  $H\beta$  is identified in emission, however, in the red,  $H\alpha$  is still strongly in emission (Figure 7) with multiple P Cygni absorption minima. The scattering wings have weakened considerably due to decreasing density in the expanding ejecta. The red wing is now measured to only  $900 \text{ km s}^{-1}$ . In addition to the O I triplet, the Ca II near-infrared triplet has appeared plus Fe II and Fe I absorption lines and the K I doublet (Figure 6). The presence of these additional absorption lines suggests that the eruption has produced the optically thick cool wind observed in several post-maximum giant eruptions such as SN2011ht (Humphreys et al. 2012) and UGC 2773 OT2009-1 (Smith et al. 2010; Foley et al. 2011), the red transients SN2008S and the NGC 300 OT, as well as the LBV/S Dor variables at maximum light. These absorption lines are offset by  $\approx 400 \text{ km s}^{-1}$  relative to the Hydrogen emission.

Several additional absorption lines from neutral metals appeared in both the blue and the red spectra from Day 99. We note that the absorption lines present earlier show a redwards shift by about  $50 - 100 \text{ km s}^{-1}$  between Days 71 and 99. The slow moving P Cyg absorption feature shows a similar redwards shift relative to the Hydrogen emission peak. This could be due either to a slowing of the dense wind or to possible infall back to the star. A slowing of the ejecta is often attributed to collision with previous circumstellar material but, in this case, the slow moving gas will have reached only 20 AU in 99 days while the two faster winds will have expanded to 63 and 91 AU, and further if ejected earlier. The dust formation radius will depend on the properties of the star, but is typically at least  $100 - 200 \text{ AU}$  and for the infrared source it is  $\approx 100 \text{ AU}$ . So what is it colliding with?

Despite a longer integration time the blue spectrum has relatively poor S/N, although  $H\beta$  still shows absorption minima. The red spectrum is shown in Figure 6 together with the Day 71 spectrum. For comparison, the three  $H\alpha$  profiles are shown together in Figure 7.

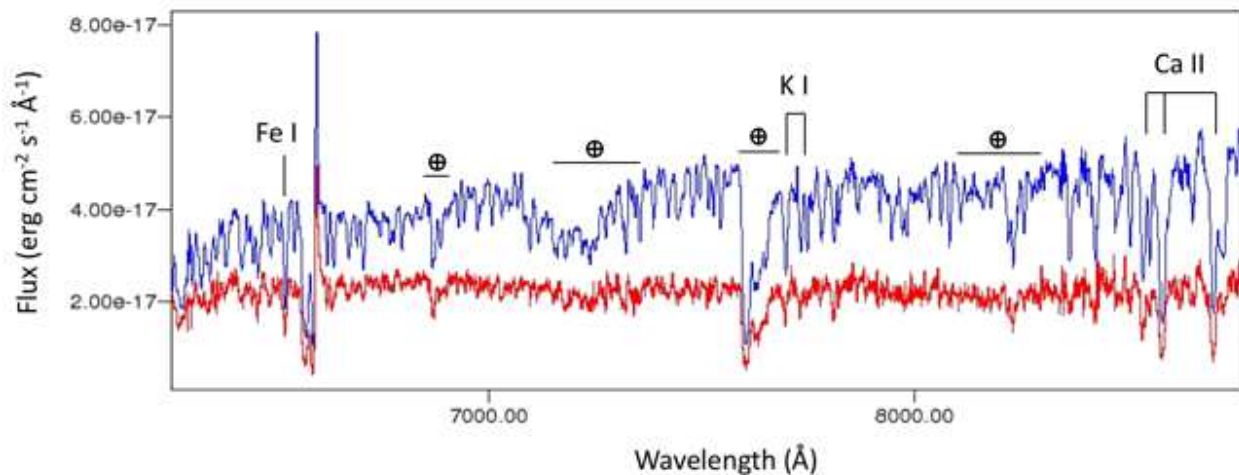


Fig. 6.— The red spectra from Days 71 (red) and 99 (blue) illustrating the development of the absorption lines.

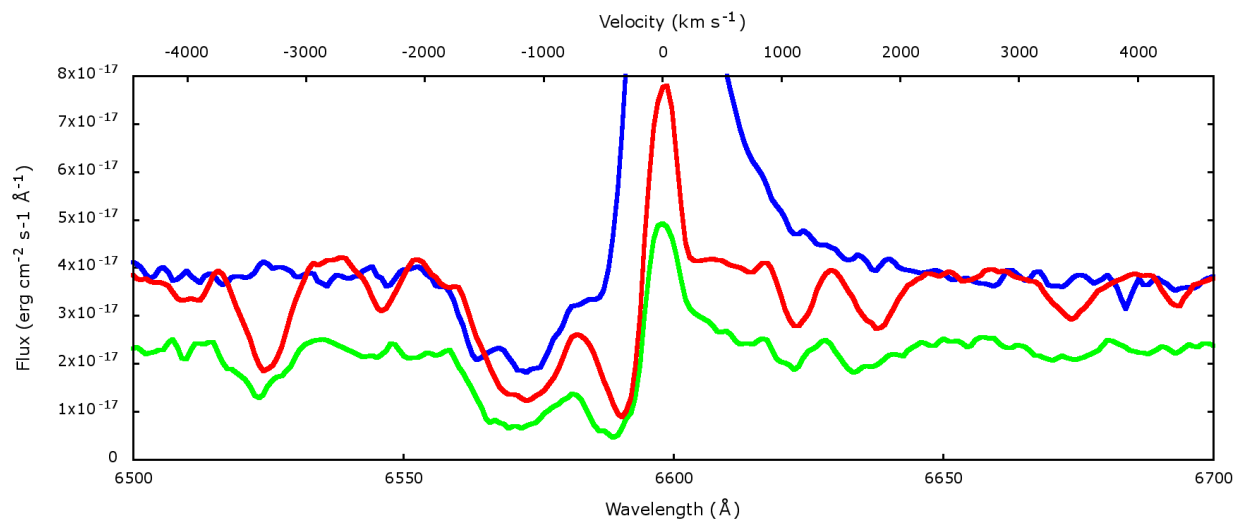


Fig. 7.— The  $H\alpha$  profiles from all three spectra illustrating the P Cygni absorption shift to longer wavelengths with time. The top spectrum (blue) is from Day 6, green from Day 71 and red from Day 99.

In general the spectra of PSN J09132750+7627410 are typical of non-terminal giant eruptions with strong narrow Hydrogen emission, Thomson scattering profiles due to the strong wind, and expansion velocities of a few  $100 \text{ km s}^{-1}$ . The distinguishing characteristic of our spectra of this eruption however, are the multiple P Cygni absorption features present in several of the Balmer lines. The outflow velocities measured for the P Cygni absorption

components from our three spectra are summarized in Table 5.

Three distinct blue-shifted absorption features or minima are present at  $H\beta$ ,  $H\gamma$  and  $H\delta$  in the spectra from Day 6 with blue-shifted velocities relative to their corresponding emission peaks at  $\sim -400$ ,  $-1100$  and  $-1600$   $\text{km s}^{-1}$ , hereafter respectively called velocity components  $a$ ,  $b$ , and  $c$ , see Figure 5. The two highest velocity minima,  $b$  and  $c$ , are clearly present at  $H\alpha$ ; component  $a$ , at the lowest velocity is very likely covered by the scattering wing.  $\text{He I}$  shows a classical P Cygni profile, although component  $c$  may be present as an unidentified absorption at  $3968\text{\AA}$ . Unfortunately, only the red spectrum from Day 71 has sufficient signal to noise for reliable line measurements. The wings on the  $H\alpha$  scattering profile have weakened considerably, and velocity component  $a$  is now clearly visible as a strong P Cygni feature. The two higher velocity minima,  $b$  and  $c$ , have weakened, and have merged into a single absorption feature although multiple components or structure are visible in the profile. In our third spectrum from Day 99, the highest velocity component  $c$  is no longer recognizable at  $H\alpha$ . There are now two strong absorption features and the blue edge of the high velocity component has shifted noticeably redwards. Two absorption minima corresponding to components  $a$  and  $b$  can still be clearly identified in the  $H\beta$  P Cygni profile and component  $c$  may still be present but much weaker.

The multiple absorption features or P Cygni profiles could be due either to multiple outflows or ejections with different velocities and energies from the current eruption or be a remnant of the wind and prior mass loss episodes of the progenitor. If we assume that the lowest velocity feature at  $-400$   $\text{km s}^{-1}$  is formed in the expanding ejecta in the current outburst, then there is clear evidence for two additional, separate winds or outflows. Their possible origin and implications for the eruption are discussed in the next section.

#### 4. Discussion

The absorption minima at  $\sim -400$   $\text{km s}^{-1}$  plus the velocity difference between the absorption lines and emission peaks of  $300\text{--}400$   $\text{km s}^{-1}$ , and the FWHM of the narrow emission cores are all consistent with a relatively slow ejection velocity which we associate with the current brightening or eruption and the formation of the cool, dense wind. Expansion velocities on this order are higher than measured for LBV/S Dor variables ( $100 - 200$   $\text{km s}^{-1}$ ) in their optically dense wind state or maximum light, but are observed in giant eruptions such as UGC 2773 OT1009-1 ( $350$   $\text{km s}^{-1}$ ) and SN2009ip ( $550$   $\text{km s}^{-1}$ ) (Smith et al. 2010; Foley et al. 2011), SN2011ht  $500 - 600$   $\text{km s}^{-1}$  (Humphreys et al. 2012) and even  $\eta$  Car ( $600$   $\text{km s}^{-1}$ ), although higher velocities have been reported in impostor eruptions such as SN2000ch ( $3000$   $\text{km s}^{-1}$ ) (Pastorello et al. 2010). The outstanding question is the origin of

the two higher velocity blue-shifted absorption minima,  $b$  and  $c$ , in PSN J09132750+7627410.

We have identified four other objects in which multiple absorption minima have been observed; SN2005gj (Trundle et al. 2008), SN2009ip (Margutti et al. 2014) and two giant eruptions, SN2000ch (Pastorello et al. 2010) and SNHunt 248 (Mauerhan et al. 2015). Trundle et al. (2008) measured velocities of 300 and 100 km s<sup>-1</sup> in two absorption troughs in the H $\alpha$  and H $\gamma$  lines in SN2005gj which they suggested were the remnants of the progenitor’s previous mass loss state as an LBV. In contrast, much higher velocities of 3000 and 5300 km s<sup>-1</sup> were measured in two absorption minima in the H $\beta$  line during SN2000ch’s 2009-OT1 eruption (Pastorello et al. 2010), and similar minima appear to be present in the H $\gamma$  line. Although, Mauerhan et al. (2015) did not specifically discuss them, multiple absorption minima can be seen in their first spectrum of SNHunt 248 for which they suggest an average outflow of  $\sim$  1200 km s<sup>-1</sup>. In the peculiar SN2009ip multiple absorptions at high velocities are observed in the post-terminal eruption spectra, but were not reported in its prior eruptions when it was considered a non-terminal giant eruption.

It is common in work on SN impostors and even terminal Type IIIn SNe, to assume that evidence for additional outflows in their spectra or mass loss episodes in the ejecta are from separate preceding events. In several of these objects, SN2011ht, SN2009ip, SN1994W, SN2009kn, etc., enhanced mass loss precedes the main eruption by only a few months or years, as in SN2009ip. Instead of being viewed as entirely separate events occurring years or decades before, they could all be part of the same instability producing more than one eruption as part of the on-going episode or instability. In the case of slow moving ejecta, it is often assumed that it is due to a prior LBV/S Dor stage and that the progenitor was an LBV, but that might not be correct. In all of these cases we do not have a sufficient timeline to know.

In PSN J09132750+7627410, the velocities at  $b$  and  $c$  are too high to be produced by the slow, dense wind of a presumed LBV progenitor or even LBVs in quiescence which have relatively slow winds for their corresponding hot supergiant spectral types. If either of these high velocity components are remnants of the progenitor’s wind, then they imply a hot star. One of these components could be the remnant of the progenitor’s wind and the second from a previous, and relatively recent, high mass loss episode. These high wind velocities are measured in late O-type and early B-type stars (Kudritzki & Puls 2000), but neither star A or B has an SED suggestive of hot star, and if the infrared source is the progenitor, the embedded star was most likely a cool or intermediate temperature supergiant.

Alternatively, both may be from previous high mass loss episodes. Their much higher expansion velocities compared to the current event suggest much more energetic eruptions. Unfortunately there is no record of prior brightenings. However, the infrared source was

observed for five years and was still present slightly more than a year prior to the eruption. If it was the progenitor, this may set a limit on when the prior ejections occurred, and an eruption, represented perhaps by one or both of these higher velocity outflows was responsible for the dust destruction. The dust condensation distance for the 780°K infrared source is 100 AU. Velocity components  $c$  and  $b$  would have reached this distance in a fraction of a year.

Here we suggest that the multiple P Cygni profiles were all formed during the current eruption which may have begun several weeks or even months before the brightening was observed, and are due to material ejected at different velocities or energies and possibly at different times.  $\eta$  Car provides an example of ejecta expanding at a range of velocities from the same giant eruption; from 600 km s<sup>-1</sup> in the Homunculus lobes to 1000 – 3000 km s<sup>-1</sup> in the outer ejecta (Weis (2012) and references therein). This possibility for PSN J09132750+7627410 is supported by the weakening and disappearance of the highest velocity component  $c$  as the eruption subsided and the ejecta expanded over the 99 days covered by our spectra.

Formation during a single mass loss episode applies just as well to the two non-terminal objects described above. The multiple P Cyg minima in the first SNHunt 248 spectrum closely resemble the absorption troughs in our first spectrum of PSN J09132750+7627410, and were not apparent in the later spectra observed over the next month. Although most had lower resolution, one with higher resolution confirms that P Cygni minima were not present about one month after they were first observed. A series of spectra by Kankare et al. (2015) shows a lack of multiple minima at the same time in their highest resolution spectrum. Thus, the multiple P Cyg absorptions quickly disappeared and could have a common origin as multiple ejections during the high mass loss event. The velocities measured in SN2000ch during its 2009-OT1 eruption seem high compared to these other objects, but are comparable to the velocities reported in  $\eta$  Car’s outer ejecta. Like SNHunt 248, the P Cyg absorptions are gone in spectra obtained a few weeks later. SN2005gj is considered to be a terminal explosion, but that doesn’t rule out the ejection of material shortly before the eruption. SN2009ip is an example where lesser “giant eruptions” occurred several times during the three years prior to what is assumed to be the final event. The multiple absorptions observed in its post-maximum spectra with very high velocities of -5000 to -12000 km s<sup>-1</sup>, were produced during its final eruption and are considered evidence for separate asymmetric outflows (Margutti et al. 2014). Similar processes may be occurring in the less energetic eruptions in the impostors. They did in  $\eta$  Car.

In the two non-terminal giant eruptions, the multiple absorption minima weaken and disappear within a few weeks. In PSN J09132750+7627410 they were present for a couple of

months. So it is possible that the evidence for multiple outflows during the high mass loss episodes is more common than has been reported due to their relatively brief or transient appearance, and to lower spectral resolution, especially in the early post-discovery spectra, as we found for PSN J09132750+7627410.

We thank Kris Davidson for valuable discussion and suggestions. Research by R. Humphreys and M. Gordon on massive stars is supported by the National Science Foundation AST-1109394. J. C. Martin’s collaborative work on luminous variables is supported by the National Science Foundation grant AST -1108890. Some of the data presented in this paper were obtained from the Mikulski Archive for Space Telescopes (MAST). STScI is operated by the Association of Universities for Research in Astronomy, Inc., under NASA contract NAS5-26555. We also used data from the Pan-STARRS Survey for Transients. Operation of the Pan-STARRS1 telescope is supported by the National Aeronautics and Space Administration under Grant No. NNX12AR65G and Grant No. NNX14AM74G issued through the NEO Observation Program.

*Facilities:* LBT/MODS1

## REFERENCES

- Atkinson, J. W., Collett, J. L., Marconi, A. et al. 2005, MNRAS, 359, 504
- Blommaert, J. A. D. L., van der Veen, W. E. C. J., van Langevelde, H. J., Habing, H. J., & Sjouwerman, L. O. 1998, A&A, 329, 991
- Bond, H. E., Bedin, L. R., Bonanos, A. Z., et al. 2009, ApJ, 695, L154
- Dolphin, A. E. 2000, PASP, 112, 1383
- Foley, R., Berger, E, Fox, O., et al. 2011, ApJ, 732, 32F
- Humphreys, R. M. & Davidson, K. 1994, PASP, 106, 1025
- Humphreys, R.M., Bond, H. E., Bedin, L. R. et al. 2011, ApJ, 743, 118
- Humphreys, R. M., Davidson, K., Jones, T. J., et al. 2012, ApJ, 760, 93
- Humphreys, R. M. & Gordon, M. S. 2015, The Astronomer’s Telegram, 7172
- Jones, T. J., Hyland, A. R., Gatley, I. & Caswell, J. L. 1982, ApJ, 253, 208
- Kankare, E., Kotak, R., Pastorello, A. et al. 2015, A&A, 581L, 4



- Khan, R., Kochanek, C. S., Stanek, K. Z. & Gerke, J. 2015, *ApJ*, 799, 187
- Kudritzki, R.-P. & Puls, J. 2000, *ARA&A*, 38, 613
- Lang, D., Hogg, D. W., Mierle, K., Blanton, M., & Roweis, S. 2010, *AJ*, 139, 1782
- Margutti, R., Milisavljevic, D., Soderberg, A. M., et al. 2014, *ApJ*, 780, 21M
- Martin, J. C., Hamsch, F.-J., Margutti, R., Tan, T. G., Curtis, I., & Soderberg, A. 2015, *AJ*, 149, 9
- Mauerhan, J. C., Van Dyk, S. D., Graham, M. L., et al. 2015, *MNRAS*, 447, 1922
- Pastorello, A., Botticella, M. T., Trundle, C., et al. 2010, *MNRAS*, 408, 181
- Pastorello, A., Cappellaro, E., Inserra, C. et al. 2013, *ApJ*, 767, 1
- Schlafly, E. F. & Finkbeiner, D. P. 2011, *ApJ*, 737, 103S
- Smith, N. et al. 2009, *ApJ*, 697, 49
- Smith, N., Miller, A., Li, W., et al. 2010, *AJ*, 139, 1451
- Tartaglia, L., Pastorello, A., Benetti, S., et al. 2015, *The Astronomer's Telegram*, 7051
- Thompson, T. A., Prieto, J. L., Stanek, K. Z., Kistler, M. D., Beacom, J. F. & Kochanek, C. S. 2009, *ApJ*, 705, 1364
- Tonry, J. L., Stubbs, C. W., Lykke, K. R., et al. 2012, *ApJ*, 750, 99T
- Toone, J. 2005, *Journal of the American Association of Variable Star Observers (JAAVSO)*, 34, 76
- Trundle, C., Kotak, R., Vink, J. S., & Meikle, W. P. S. 2008, *A&A*, 483, L47
- Van Dyk, S. D., Peng, C. Y., King, J. Y. et al. 2000, *PASP*, 112, 1532
- Van Dyk, S. D. & Matheson, T. 2012, in *Eta Carinae and the Supernova Impostors*, *Astrophys. & Sp. Sci. Library* 384 (ed. K. Davidson & R.M. Humphreys, Springer Media, New York), 249
- Weis, K. 2012, in *Eta Carinae and the Supernova Impostors*, *Astrophys. & Sp. Sci. Library* 384 (ed. K. Davidson & R.M. Humphreys, Springer Media, New York), 171
- Zacharias, N., Finch, C. T., Girard, T. M., et al. 2013, *AJ*, 145, 44

---

This preprint was prepared with the AAS L<sup>A</sup>T<sub>E</sub>X macros v5.2.

Table 1. Journal of Spectroscopic Observations

UT Date	Instrument	Exp. Time	Wavelength	Reference
11.98 Feb 2015 (Day 1)	Asiago 1.8m	...	3400 – 8200 $\text{\AA}$	Tartaglia, et al. (2015)
16.24 Feb 2015 (Day 6)	LBT/MODS1	30m	3200 $\text{\AA}$ – 1 $\mu\text{m}$	
22.13 Apr 2015 (Day 71)	”	30m	”	
20.16 May 2015 (Day 99)	”	60m	”	

Table 2. Multi-color Photometry

U.T. Date	B mag	V mag	r(P1) mag	R mag	i(P1) mag	I mag	Comment
10.92 Feb 2015	...	...	...	...	...	...	18.0 unfiltered; Cortini
11.15 Feb 2015	...	...	...	...	...	...	17.7 unfiltered; Yusa
11.23 Feb 2015	...	18.14	...	...	...	17.42	Kiyota
11.43 Feb 2015	...	...	...	...	...	...	17.8 unfiltered; Noguchi
11.98 Feb 2015	...	18.7	...	...	...	...	Tartaglia, et al. (2015)
26.91 Feb 2015	...	...	18.34 $\pm$ 0.03	...	...	...	Pan-STARRS
12.66 Mar 2015	18.83 $\pm$ 0.08	18.58 $\pm$ 0.12	...	17.54 $\pm$ 0.05	...	...	Barber Obs.
17.63 Mar 2015	18.69 $\pm$ 0.11	18.22 $\pm$ 0.12	...	17.58 $\pm$ 0.05	...	17.40 $\pm$ 0.09	Barber Obs.
28.76 Mar 2015	...	...	...	...	18.80 $\pm$ 0.02	...	Pan-STARRS
03.82 Apr 2015	...	...	...	...	18.94 $\pm$ 0.03	...	Pan-STARRS
29.60 Apr 1015	>18.8	> 18.9	...	>18.5	...	...	Barber Obs
19.67 May 2015	> 19.0	> 19.3	...	18.22 $\pm$ 0.09	...	...	Barber Obs
13.73 Jan 2016	> 19.2	>19.0	...	>18.6	...	...	Barber Obs
5.15 Feb 2016	>19.5	> 19.2	...	>18.8	...	...	Barber Obs

Table 3. HST/WFPC2 and Spitzer/IRAC Photometry

Date	Star	F450W mag.	F814W mag.	3.6 $\mu$ m mag.	4.5 $\mu$ m mag.	ICRS J2000 Position
6 Jul 2001	A	$24.43 \pm 0.20$	$23.79 \pm 0.15$	...	...	9:13:27.48 +76:27:41.1
"	B	$26.08 \pm 1.28$	$24.00 \pm 0.18$	...	...	9:13:27.38 +76:27:40.9
2 Dec 2009	...	...	...	$19.41 \pm 0.3$	$18.40 \pm 0.3$	...
12 Apr 2010	...	...	...	$19.16 \pm 0.2$	$18.65 \pm 0.3$	...
25 Jan 2014	...	...	...	$19.21 \pm 0.2$	$18.32 \pm 0.1$	9:13:27.24 +76:27:41.2

Table 4. Line Identifications and Measured Velocities in PSN J09132750+7627410

Line	Velocity km s <sup>-1</sup>	P Cyg Vel. km s <sup>-1</sup>	Blue-Edge Vel. km s <sup>-1</sup>	Red Wing km s <sup>-1</sup>
Day 6 (16 Feb 2015)				
Emission Lines				
H $\alpha$	1607	... , -1137, -1537	... , -1337, -1817	2460
H $\beta$	1648	-466, -1154, -1559	-681, -1353, -1946	2200
H $\gamma$	1680	-412, -1027, -1622	-646, -1127, -1876	1650
H $\delta$	1745	-426, -1124, -1670	-717, -1255, -1953	1668
H $\epsilon$	1745	-428, ... , ... <sup>a</sup>	... , ... , ...	
Fe II(42) 4923.9Å	1682	-409	...	...
Fe II(42) 5018.4Å	1680	-348	...	...
Fe II(42) 5169.0Å	1706	-427	...	...
Absorption lines				
H 3889Å	1365	...	...	...
H 3835Å	1408	...	...	...
H 3797Å	1335	...	...	...
H 3770Å	1313	...	...	...
Ca II K	1391	...	...	...
O I 7774Å	1397	...	...	...
Day 71 (22 Apr 2015)				
Emission Lines				
H $\alpha$	1595	-396, -1171, -1453::	-727, -1764	914
Absorption lines				
O I 7774Å	1389	...	...	...
Ca II8498Å	1239	...	...	...
Ca II8542Å	1296	...	...	...
Ca II8662Å	1306	...	...	...
K I 7665Å	1211	...	...	...
K I 7699Å	1230	...	...	...
Fe II 6432Å	1240	...	...	...
Fe I 6494Å	1289	...	...	...
Day 99 (20 May 2015)				
Emission Lines				
H $\alpha$	1614	-364, -1161, ...	-682, -1735	909
H $\beta$	1651	-316, -913, range	-636, -1047,	...
H $\gamma$	1701	...	...	...

Table 4—Continued

Line	Velocity km s <sup>-1</sup>	P Cyg Vel. km s <sup>-1</sup>	Blue-Edge Vel. km s <sup>-1</sup>	Red Wing km s <sup>-1</sup>
Absorption lines				
O I 7774Å	1420	...	...	...
Ca II 8498Å	1318	...	...	...
Ca II 8542Å	1333	...	...	...
Ca II 8662Å	1340	...	...	...
K I 7665Å	1295	...	...	...
K I 7699Å	1341	...	...	...
Fe II 6432Å	1288	...	...	...
Fe I 6494Å	1366	...	...	...
Fe I 8327Å	1329	...	...	...
Fe I 8387Å	1283	...	...	...
Na I 8194Å	1333	...	...	...

<sup>a</sup>An unidentified line at 3968Å may be the blue-shifted component c with a corresponding velocity of -1773 km s<sup>-1</sup>.

Table 5. Summary of the Outflow Velocities

Date	Velocity km s <sup>-1</sup>	Lines
Day 6	-433	H $\beta$ , H $\gamma$ , H $\delta$ , H $\epsilon$
	-1110	H $\alpha$ , H $\beta$ , H $\gamma$ , H $\delta$
	-1597	H $\alpha$ , H $\beta$ , H $\gamma$ , H $\delta$
	-395	Fe II (42)
Day 71	-396	H $\alpha$
	-1171	H $\alpha$
	-1453	H $\alpha$
Day 99	-340	H $\alpha$ , H $\beta$
	-1161, -913	H $\alpha$ , H $\beta$